PERGAMON

Chemical Engineering Science 56 (2001) 6295–6302

Chemical Engineering Science

www.elsevier.com/locate/ces

Modeling of hydrodynamic cavitation reactors: a unified approach

V. S. Moholkar[a, *], A. B. Pandit[b]

[a] *Department of Chemical Engineering, University of Twente, P.O. Box 217, NL - 7500 AE Enschede, The Netherlands*
[b] *Chemical Engineering Division, University Department of Chemical Technology, University of Mumbai, Mumbai 400 019, India*

Abstract

An attempt has been made to present a unified theoretical model for the cavitating flow in a hydrodynamic cavitation reactor using the nonlinear continuum mixture model for two-phase flow as the basis. This model has been used to describe the radial motion of bubble in the cavitating flow in two geometries in hydrodynamic cavitation reactors, viz., a venturi tube and an orifice plate. Simulations of the bubble dynamics in a venturi flow demonstrate the stable oscillatory radial bubble motion due to a linear pressure gradient. Due to an additional pressure gradient due to turbulent velocity fluctuations the radial bubble motion in case of an orifice flow is a combination of both stable and oscillatory type. The results of numerical simulations have been explained on the basis of analogy between hydrodynamic cavitation and acoustic cavitation.

Keywords: Bubble dynamics; Two-phase flow; Hydrodynamic cavitation; Acoustic cavitation; Process Intensification

1. Introduction

Process industries are energy intensive. To improve the efficiency of the processes constant effort is needed to explore new ways of introducing energy into the system. Cavitation as a source of energy input for the chemical processes is increasingly being studied owing to its ability to generate high temperatures and pressures at nearly ambient bulk processing conditions. Hydrodynamic cavitation which is generated by the flow of liquid under controlled conditions through simple geometries such as venturi or orifice plates has been attempted as an alternative to the acoustic cavitation over past several years. This form of cavitation has been proved to be more efficient for large-scale operation than the acoustic cavitation in several chemical processes such as fatty oil hydrolysis (Joshi & Pandit, 1993), polymerization and depolymerization of aqueous polymeric solutions (Chivate & Pandit, 1993) and microbial cell disruption (Save, Joshi, & Pandit, 1997, 1994). A detailed discussion about diverse processes that can be carried out with hydrodynamic cavitation and the economics of hydrodynamic cavitation reactors can be found in Shah, Pandit, and Moholkar (1999). Thus hydrodynamic cavitation reactors are the new generation gas–liquid reactors which have significant potential for application in various process industries. The main physical phenomena responsible for the production of local extremes of pressure and temperature in hydrodynamic cavitation is the radial motion of the bubble driven by the varying pressure in the flow. In this paper we make an attempt to present a unified theoretical model for the bubble dynamics in hydrodynamic cavitation with different flow geometries such as venturi tube and orifice plate using the continuum mixture model (van Wijngaarden, 1968, 1972) as the basis.

2. Mathematical formulations and algorithm of simulations

The basis of the simulations done in the present work is the nonlinear continuum mixture model coupled with Rayleigh–Plesset equation proposed by van Wijngaarden (1968, 1972). The assumptions made in this analysis are as follows:

1. The liquid is assumed to be incompressible and the slip between the two phases is neglected.
2. There is no coalescence and further break up of the bubbles in the flow.

* Corresponding author. Fax: 31-053-489-3849.
E-mail address: v.s.moholkar@ct.utwente.nl (V. S. Moholkar).

0009-2509/01/$ - see front matter
PII: S0009-2509(01)00253-6

3. The density of gas and vapor is neglected in comparison to the density of the liquid.
4. All bubbles have assumed to have the same initial radius R_0.
5. The bubbles are assumed to have spherical geometry during entire lifetime.
6. Heat and mass transfer effects across the bubble wall are neglected.
7. The temperature and density gradients in the bubble interior are neglected.
8. The bubbles are assumed to be in mechanical equilibrium with the surrounding after generation.

For a gas–liquid flow with the gas bubbles of radius $R(x,t)$ and the number density n, the mass density of the mixture is written as

$$\rho = \rho_L\ (1 - nV), \tag{1}$$

where $V = 4/3\pi R^3(x,t)$. The continuity and momentum equations of the two-phase flow have the form (Wang & Brennen, 1998)

$$\frac{\partial(\rho A)}{\partial t} + \frac{\partial(\rho u A)}{\partial x} = 0, \tag{2}$$

$$\frac{\partial u}{\partial t} + u\frac{\partial u}{\partial x} = -\frac{1}{\rho}\frac{\partial p}{\partial x}. \tag{3}$$

The bubble void fraction in the flow is $\alpha(x,t) = 4/3n\pi R^3(x,t)/[1 + 4/3n\pi R^3(x,t)]$. The interaction of the bubbles with the flow is modeled by Rayleigh–Plesset equation of bubble dynamics (Plessset & Prosperetti, 1977)

$$\rho_L\left[R\frac{D^2R}{Dt^2} + \frac{3}{2}\left(\frac{DR}{Dt}\right)^2\right] = \left(P_0 + \frac{2\sigma}{R_0} - P_v\right)\left(\frac{R_0}{R}\right)^{3k} - (P_0 + P_t) - \frac{2\sigma}{R} - \frac{4\mu}{R}\left(\frac{DR}{Dt}\right) + P_v, \tag{4}$$

where $D/Dt = [\partial/\partial t + u\,\partial/\partial x]$ is the Lagrangian derivative. k is assumed to be 1 on the basis of the analysis of Hilgenfeldt, Lohse, and Brenner (1996). Eqs. (2)–(4) now represent a simple model of one-dimensional two-phase flow with the nonlinear bubble dynamics. In case of cavitating flow in geometries such as venturi tube or an orifice plate the mean flow parameters change rapidly in space and time due to acceleration/deceleration of the flow and hence the method of simple linearization is not valid. As such we adopt the approach of Wang & Brennen (1998) based on the assumption of steady state cavitating flow for a constant mass flow rate.

Modeling of the venturi flow: A simple expression for the area of a venturi with length L is

$$A(x) = \left\{1 - \frac{1}{2}\delta\left[1 - \cos\left(\frac{2\pi x}{L}\right)\right]\right\}^{-1/2} \quad \text{for } 0 \leqslant x \leqslant L. \tag{5}$$

The throat of the venturi is located at $L/2$ and the value of δ determines the throat to pipe diameter ratio. The bubbles are assumed to generate at the throat of the venturi when the pressure in the flow drops to vapor pressure of the liquid. The initial conditions for the simulations are $x = L/2$, $R = R_0$, $u = u_t$ and $\alpha = \alpha_0$. u_t can be determined by the cavitation number

$$C_i = \frac{P_2 - P_v}{1/2\rho_L u_t^2}. \tag{6}$$

Modeling of the orifice flow: In case of high Reynolds number flow past an orifice plate the velocity of the flow field has two components: the mean flow velocity and the turbulent fluctuating velocity superimposed over it. Therefore in an orifice flow the dynamics of a bubble is influenced by both the mean flow and the instantaneous turbulent velocity fluctuations. The instantaneous velocity in the turbulent flow downstream of an orifice plate is written as

$$u = U + \bar{u}'. \tag{7}$$

A detailed modeling of two-phase turbulent flow will be quite complicated. In order to simplify the problem of turbulence modeling, yet representing the physical phenomena, we follow the algorithm described in our earlier work (Moholkar & Pandit, 1997) which is based on assumption that the rate at which large eddies supply energy to the smaller eddies is proportional to the reciprocal of the time scale of the larger eddies. The amount of kinetic energy per unit mass is proportional to $\bar{u}'^2$ and the rate of transfer of energy is assumed to be $\bar{u}'/l$ where l represents the size of the largest eddies of the flow. The rate of supply of the energy, which is also equal to the rate of dissipation of energy, is $\approx \bar{u}'^2\bar{u}'/l = \bar{u}'^3/l$. The main steps of the algorithm are as follows:

1. The rate of turbulence energy dissipation per unit mass in the region of pressure recovery downstream of the orifice is estimated using the permanent pressure head loss in the flow and the volumetric flow rate assuming isotropic turbulence in the region of pressure recovery.
2. The length scale of the eddy is estimated using the Prandtl eddy model ($l = 0.08d$) in which the conduit diameter is taken as average of orifice and the pipe diameter.
3. The steady-state frequency of the turbulent fluctuation velocity f_T (i.e. the total number of oscillations of the turbulent fluctuating velocity in the region of pressure recovery, $L' = 8d_p$) is obtained by multiplying the rate of energy transfer ($\bar{u}'/l$) by the time of pressure recovery downstream of the orifice (τ) which is calculated using Newton's equations.

Now, the instantaneous fluid velocity u in Eqs. (2) and (3) for the orifice flow is written as

$$u = U + \bar{u}' \sin\left(\frac{2\pi f_T x}{L'}\right), \tag{8}$$

where the oscillatory nature of $\bar{u}'$ is approximated with a sinusoidal function. With the assumption of linear expansion of the mean flow downstream of the orifice plate, the flow area $A(x)$ is written as

$$A(x) = A_o + \left(\frac{A_p - A_o}{L'}\right) x. \tag{9}$$

The initial conditions of the simulations of the orifice flow are $x = 0$, $u = U_o$, $R = R_0$, $\alpha = \alpha_o$. U_o can be determined by cavitation number (i.e., substituting u_t by U_o in Eq. (6)).

Steady state solutions: Under assumption of steady state, equation system (2)–(4) is transformed as

$$\rho_L \left(1 - \frac{4}{3}\pi n R^3\right) uA = \text{constant}, \tag{10}$$

$$u\frac{\mathrm{d}u}{\mathrm{d}x} = -\frac{1}{\rho_L(1 - 4/3\pi n R^3)}\frac{\mathrm{d}p}{\mathrm{d}x}, \tag{11}$$

$$P_t = P_v - P_0 + \left(P_0 + \frac{2\sigma}{R_0} - P_v\right)\left(\frac{R_0}{R}\right)^{3k} - \frac{2\sigma}{R} - \frac{4\mu u}{R}\left(\frac{\mathrm{d}R}{\mathrm{d}x}\right) - \rho_L\left[R\left(u^2\frac{\mathrm{d}^2R}{\mathrm{d}x^2} + u\frac{\mathrm{d}u}{\mathrm{d}x}\frac{\mathrm{d}R}{\mathrm{d}x}\right) + \frac{3u^2}{2}\left(\frac{\mathrm{d}R}{\mathrm{d}x}\right)^2\right]. \tag{12}$$

Replacing of p in Eq. (11) by P_t gives a system of three simultaneous differential equations, which can be solved using Runge–Kutta fourth-order method with adaptive step size control (Press, Teukolsky, Flannery, & Vetterling, 1992). Due to assumption of incompressibility of the liquid the simulations are terminated at a point where the Lagrangian bubble wall velocity ($u\,\mathrm{d}R/\mathrm{d}x$) exceeds velocity of sound in water (i.e., 1500 m s^{-1}). The other physical properties of the flow are: $\rho_L = 1000$ kg m^{-3}; $\sigma = 0.072$ N m^{-1}; $\mu = 10$ cP.

3. Analogy between hydrodynamic cavitation and acoustic cavitation

In this section we try to develop an analogy between acoustic cavitation and hydrodynamic cavitation, i.e. we try to find those properties of the flow in hydrodynamic cavitation that have similar effect on the bubble motion as that of the properties of the ultrasound wave in acoustic cavitation. The two principal aspects of the radial motion of a bubble are:

1. The type of bubble motion whether a stable oscillatory type or a transient one comprising of a single growth phase followed by a violent collapse.
2. The cavitation intensity, i.e. the magnitude of the pressure and temperature pulses produced during the collapse of the bubble.

The major factors that influence the above aspects of the radial bubble motion in acoustic cavitation are (1) pressure amplitude and frequency of the ultrasound wave, and (2) maximum size reached during bubble growth.

Pressure amplitude and frequency: For low-pressure amplitudes (< 1 bar) the bubble undergoes a stable oscillatory motion. When the pressure amplitude exceeds a certain value called transient cavitation threshold the bubble undergoes an explosive growth followed by a violent collapse producing local extremes of temperature and pressure. The intensity of the collapse increases with rising pressure amplitudes (at a fixed frequency). The bubble grows in the rarefaction half-cycle of the acoustic wave and contracts (and collapses under certain conditions) in the following compression half-cycle. Although the bubble motion has a phase lag with the acoustic wave due to inertia, the period of the bubble motion is very nearly the same as that of the period of the acoustic wave. The higher the frequency of the acoustic wave (at a fixed pressure amplitude) the lesser is the growth of the bubble and hence the bubble life.

Maximum bubble size: Flynn (1975) hypothesized that for a bubble to undergo transient collapse, the ratio $R_{\max}/R_0$ during the radial motion of the bubble should exceed the minimum value. For air bubbles in water this value is ≈ 2. Above this ratio, the dynamic behavior of a bubble is controlled by the inertial forces in the liquid surrounding it and the liquid transfers an ever-increasing amount of energy to the collapsing bubble with increasing value of ratio $R_{\max}/R_0$ thus increasing the intensity of its collapse.

The analogy between acoustic cavitation and the hydrodynamic cavitation with different flow configurations is given as follows:

Venturi flow configuration: In a venturi tube the pressure of the flow recovers from the venturi throat at the expense of velocity of the flow. This change in velocity head of the flow takes place over the length of the venturi (L). For a single-phase flow the velocity in the pipe in which the venturi discharges (u_p) can also be written as $\eta^2 u_t$. Therefore, the approximate pressure gradient that drives the motion of the bubbles in the flow is $(1/2L)\rho_L(1 - \eta^2)^2 u_t^2$. The length of venturi tube over which the velocity head transformation takes place is equivalent of the frequency of ultrasound waves while the pressure gradient over the length of the venturi is equivalent of the pressure amplitude of the ultrasound waves in ultrasonic cavitation. The pressure gradient is a linearly increasing

function and hence will never tend to grow the bubble beyond its initial size. Nonetheless, a larger pressure gradient will cause higher compression of the bubble during its flow in venturi and hence higher will be the amplitude of subsequent rebounces of the bubble.

Orifice flow configuration: In this configuration, the pressure recovery in the flow takes place approximately over a length of eight pipe diameters downstream of the orifice plate where the mean velocity of the flow at the orifice (U_o) reduces to the pipe velocity (u_p). u_p can also be written as $U_o\beta^2$ for a single-phase flow past the orifice plate. The mean velocity is superimposed by the turbulent fluctuating velocity ($\bar{u}'$) which is of oscillatory nature. We denote the relative magnitude and frequency of the turbulent fluctuations as I and f_T, respectively. Therefore, the two pressure gradients that drive the bubble motion in the orifice flow are approximated as

1. The mean pressure gradient $(1/2L')\rho_L(1-\beta^2)^2U_o^2$ defined in a similar way as in case of venturi.
2. The turbulent pressure gradient $(I) \approx (1/2)\rho_L\bar{u}'^2$.

The equivalent of frequency in acoustic cavitation has also two components:

1. The length of the region of pressure recovery downstream of the orifice plate (L').
2. The frequency of the turbulent velocity fluctuations (f_T).

Unlike the mean pressure gradient the turbulent pressure gradient (due to its oscillatory nature) will grow the bubble due to reduction in the mean pressure during its negative oscillations. Hence the bubble motion in orifice flow depends on the resultant of these two gradients.

4. Results and discussion

Simulations were carried out to assess the effect of several design parameters on the bubble motion in the cavitating flow in two different flow geometries: a venturi tube and an orifice plate. We would like to specifically mention that the cavitating flow in a venturi or downstream of an orifice plate is not necessarily stable for all operating parameters and can flash to vapor under certain conditions. While choosing the simulation parameters in the present work we have checked the stability criterion given by Wang & Brennen (1998) a priori.

4.1. Simulations of a venturi flow

Effect of recovery or upstream pressure: The conditions for the simulations are given in caption of Fig. 1. It can be seen that the radial motion of the bubble in a venturi flow is stable oscillatory type. The amplitude of the oscillations of the bubbles and hence the magnitude of the resultant pressure pulses increases with the recovery pressure. This effect can be ascribed to the rise in pressure gradient in the venturi flow with rise in recovery pressure for a fixed length of the venturi tube.

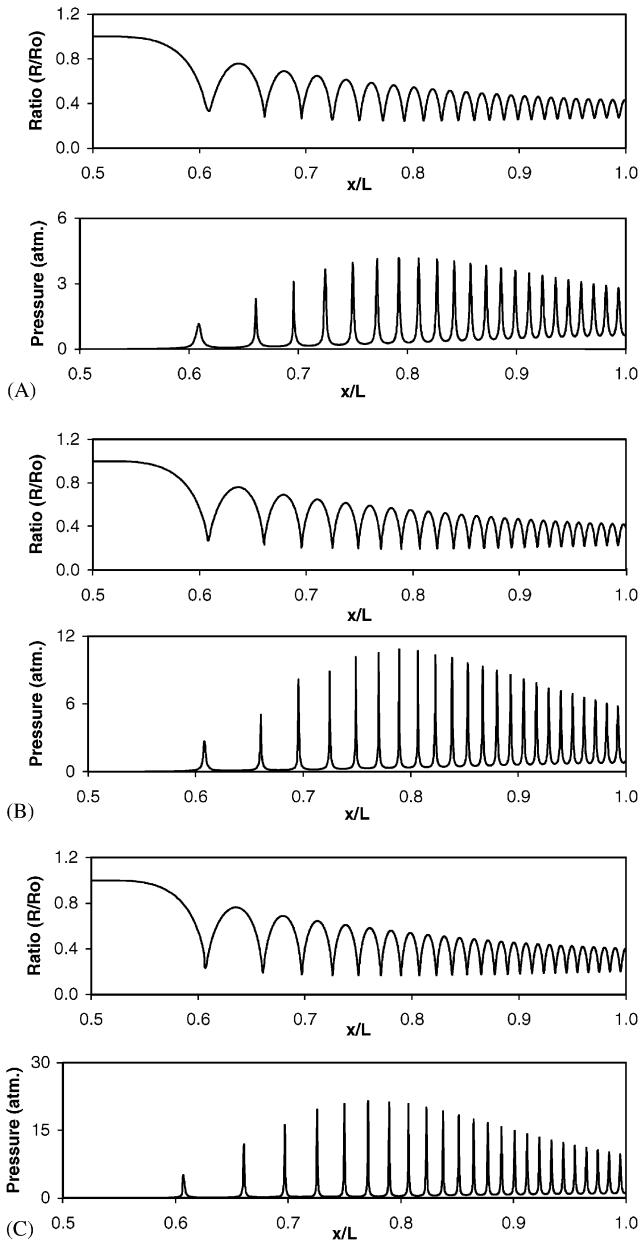

Fig. 1. Effect of recovery pressure on the bubble dynamics in venturi flow: radius history and pressure pulses of bubble oscillations. Parameters for simulations: (A) $P_2 = 1$ bar; (B) $P_2 = 1.5$ bar; (C) $P_2 = 2$ bar. Other parameters: $\eta = 0.84$, $\alpha_0 = 2 \times 10^{-6}$, $C_i = 1$, $R_0 = 100$ μm, $L = 0.1$ m.

Effect of length of venturi: The conditions and results of the simulations are given in Fig. 2. It can be inferred from Fig. 2 that a reduction in length of the venturi for a fixed recovery pressure increases the amplitude of

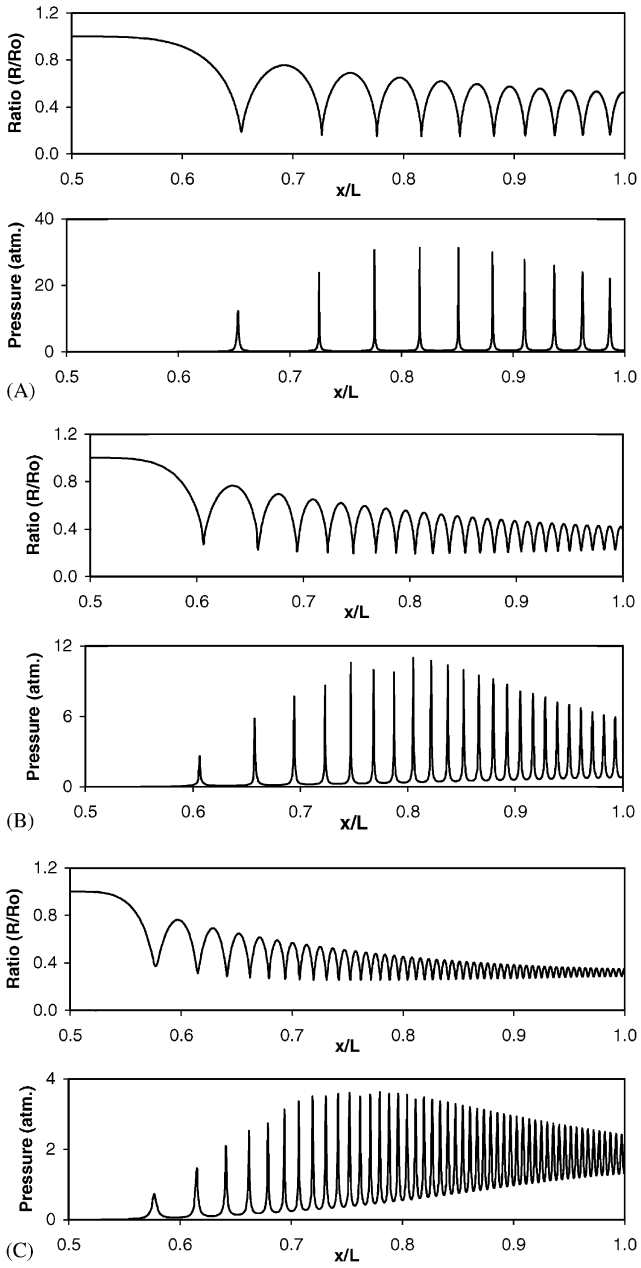

Fig. 2. Effect of length of venturi tube on the bubble dynamics in venturi flow: radius history and pressure pulses of bubble oscillations. Parameters for simulations: (A) $L = 0.05$ m; (B) $L = 0.1$ m; (C) $L = 0.2$ m. Other parameters: $\eta = 0.84$, $\alpha_0 = 2.5 \times 10^{-6}$, $C_i = 1$, $R_0 = 100$ μm, $P_2 = 1$ bar.

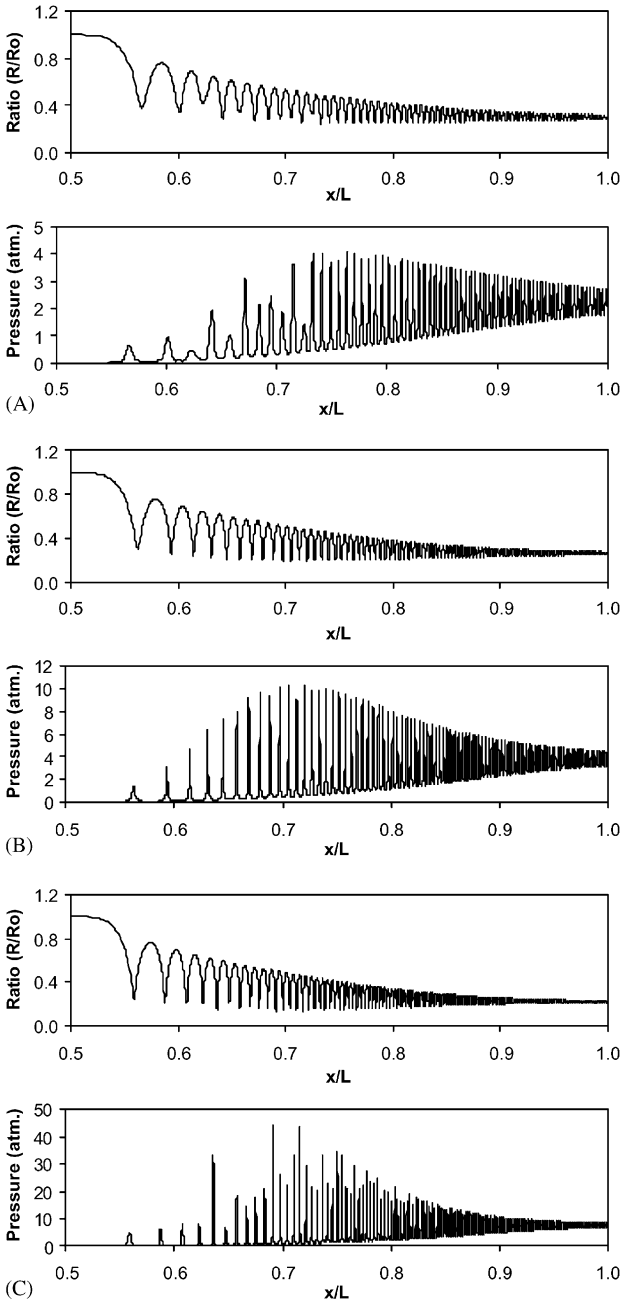

Fig. 3. Effect of venturi throat to pipe diameter ratio on the bubble dynamics in venturi flow: radius history and pressure pulses of bubble oscillations. Parameters for simulations: (A) $\eta = 0.84$; (B) $\eta = 0.78$; (C) $\eta = 0.69$. Other parameters: $P_2 = 1$ bar, $\alpha_0 = 2 \times 10^{-6}$, $C_i = 0.9$, $R_0 = 100$ μm, $L = 0.1$ m.

the oscillatory motion of the bubble. This effect can also be attributed to the rise in the pressure gradient driving the radial bubble motion in the flow with reduction in the length of the venturi for a fixed recovery pressure.

Effect of venturi throat to pipe diameter ratio: Fig. 3 depicts the conditions and results of the simulations. It can be deduced from Fig. 3 that a reduction in η causes a significant rise in the intensity of the oscillation of the bubble in the cavitating flow. Like in the two cases above, this result is also an effect of the alteration in the pressure gradient driving the radial bubble motion with decreasing η. As explained in Section 3 the lesser the value of η (for fixed values of P_2 and L); the larger is the pressure gradient that causes the observed changes in the radial dynamics of the bubble.

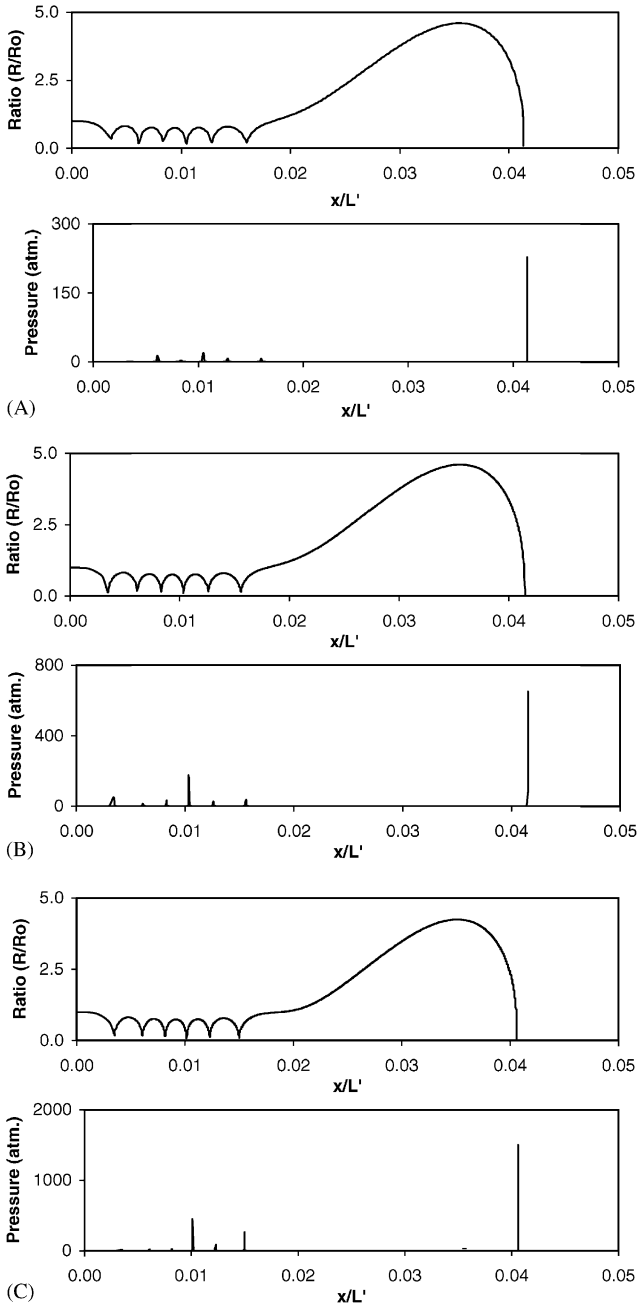

Fig. 4. Effect of recovery pressure on the bubble dynamics in orifice flow: radius history and pressure pulses of bubble oscillations. Parameters for simulations: (A) $P_2 = 1$ bar ($I = 0.02$ bar, $f_T = 30.3$); (B) $P_2 = 2$ bar ($I = 0.04$ bar, $f_T = 30.3$); (C) $P_2 = 3$ bar ($I = 0.06$ bar, $f_T = 30.3$). Other parameters: $\beta = 0.5$, $\alpha_o = 2 \times 10^{-6}$, $C_i = 1$, $R_0 = 100$ μm, $d_p = 0.05$ m.

4.2. Simulations of an orifice flow

Effect of the recovery pressure: The parameters and results of the simulations are given in Fig. 4. Fig. 4 indicates that initially the bubble undergoes a small amplitude oscillatory motion followed by a growth and transient collapse. It is clear that during the initial stages

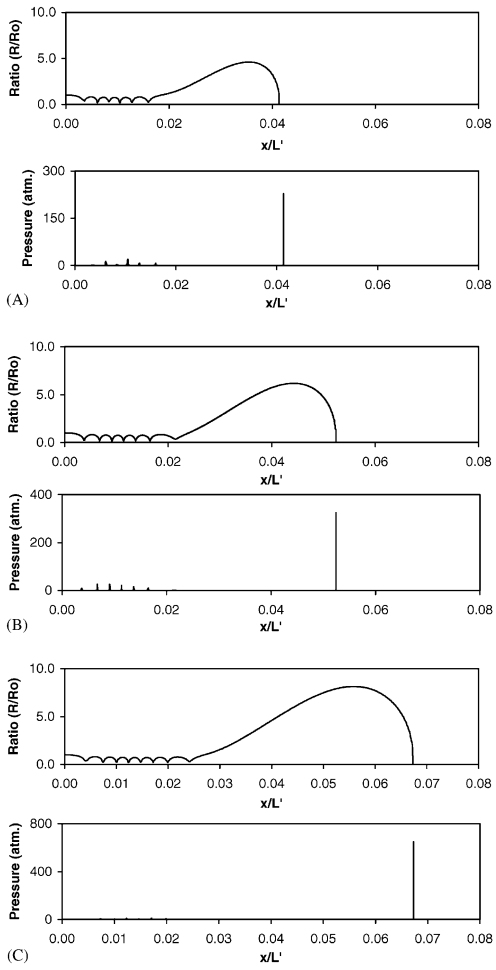

Fig. 5. Effect of orifice to pipe diameter ratio on the bubble dynamics in orifice flow: radius history and pressure pulses of bubble oscillations. Parameters for simulations: (A) $\beta = 0.5$ ($I = 0.02$ bar, $f_T = 30.3$); (B) $\beta = 0.6$ ($I = 0.018$ bar, $f_T = 25.3$); (C) $\beta = 0.7$ ($I = 0.015$ bar, $f_T = 20.5$). Other parameters: $P_2 = 1$ bar, $\alpha_0 = 2 \times 10^{-6}$, $C_i = 1$, $R_0 = 100$ μm, $d_p = 0.05$ m.

of the developing flow downstream of the orifice the mean pressure gradient dominates the bubble motion. Although the intensity of the initial oscillatory motion of the bubble grows with rising recovery pressure, the growth of the bubble thereafter is not affected since the frequency of the turbulent pressure fluctuations stays the same. Explanations for these effects follow from the analogy given in Section 3. Nonetheless, during the transient collapse, which occurs during the positive oscillation of the turbulent pressure gradient, the mean and turbulent pressure gradient sum up their effect thus making the collapse of the more intense with rising recovery pressure.

Effect of orifice to pipe diameter ratio: The results of the simulations along with the parameters for simulations are given in Fig. 5. The distinct effect of rise in orifice to pipe diameter ratio on the bubble motion is that the maximum size reached during oscillation and the intensity of the collapse of the bubble increases. Any change in β

does not cause much change either in the mean pressure gradient or the magnitude of the turbulent pressure fluctuations but significantly reduces the frequency of the turbulent velocity fluctuations. Therefore, the bubble grows to a larger size under the influence of turbulent pressure fluctuations with reduced frequency. A larger size at the beginning of the collapse also results in higher cavitation intensity as outlined in Section 3.

Effect of the pipe size: The conditions and the results of simulations are given in Fig. 6. Two marked effects of rise in pipe diameter on bubble motion are evident: (1) the number of small amplitude oscillations of the bubbles and hence the pressure pulses resulting out of them decreases although the number of oscillations that the bubble completes before undergoing the transient growth increases, and (2) the maximum size of the bubble reached during the transient growth and hence the intensity of the collapse of the bubbles increases. An increase in the pipe size causes an increase in the length of region of pressure recovery. This reduces the mean pressure gradient significantly and thus the motion of the bubble is essentially governed by the turbulent pressure fluctuations. As such the bubble grows to a larger size before undergoing a transient collapse which results in increment in the cavitation intensity for the reasons explained in Section 3.

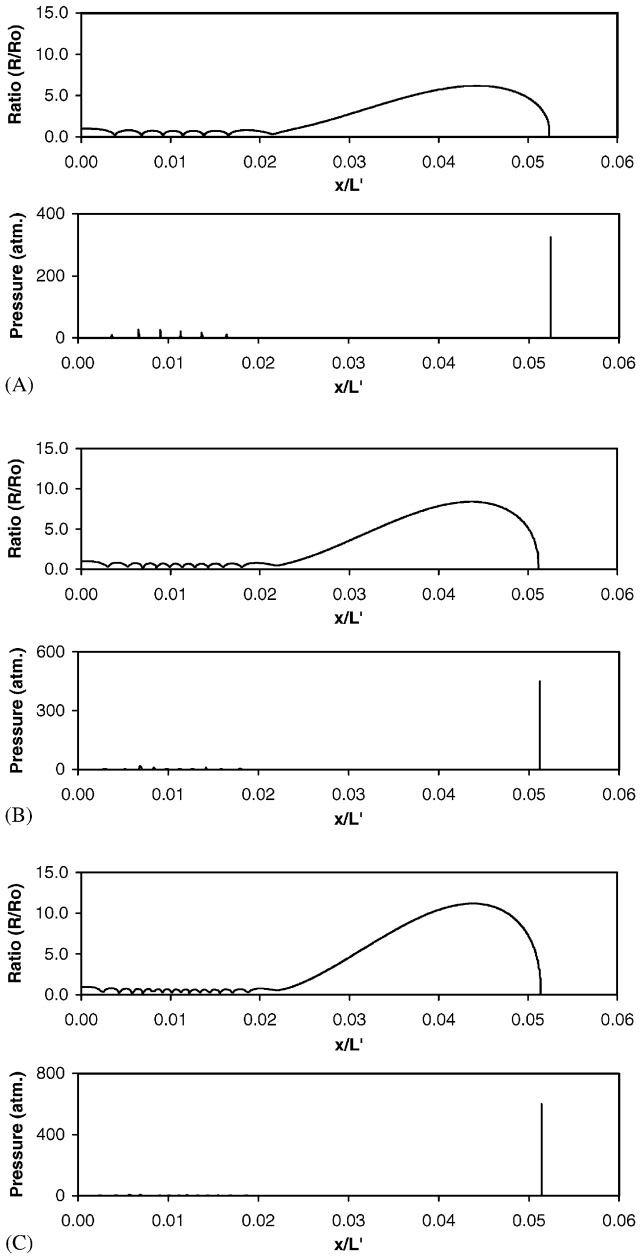

Fig. 6. Effect of pipe size on the bubble dynamics in orifice flow: radius history and pressure pulses of bubble oscillations. Parameters for simulations: (A) $d_p = 0.05$ m ($I = 0.018$ bar, $f_T = 25.3$); (B) $d_p = 0.075$ m ($I = 0.018$ bar, $f_T = 25.3$); (C) $d_p = 0.1$ m ($I = 0.018$ bar, $f_T = 25.3$). Other parameters: $P_2 = 1$ bar, $\alpha_0 = 2 \times 10^{-6}$, $C_i = 1$, $R_0 = 100$ μm, $\beta = 0.6$.

5. Conclusion

The present work reports numerical simulations of the bubble dynamics in two flow geometries used in hydrodynamic cavitation reactors, viz. venturi tube and orifice plate using nonlinear continuum mixture model. Despite of several simplifying assumptions made in the analysis the simulations represent some interesting features of the bubble motion in the cavitating flow. The radial motion of the bubble in the cavitating flow in venturi is of stable oscillatory type. The bubble motion in the orifice flow is found to be a combination of stable oscillatory motion and a transient motion (resembling the bubble motion in acoustic cavitation) as a result of two pressure gradients of different type, viz. the linear mean pressure gradient and the oscillatory turbulent pressure gradient. As such, the cavitation intensity produced in an orifice flow is of much higher magnitude than that in a venturi flow.

The simulations reported in this work establish definite trends in the cavitation intensity produced in the hydrodynamic cavitation reactor with the design parameters, which can form a basis for the optimization of the hydrodynamic cavitation reactors. In addition the model presented in this work can also predict the magnitudes of the temperature and pressure pulses for a given set of design parameters. Based on the simulations presented several strategies for the optimization of hydrodynamic cavitation reactor can be proposed:

1. An orifice flow configuration is suitable for only intense chemical reactions. For milder processes (typically between 10 and 25 bar) a venturi configuration is suitable.
2. In case of venturi flow the most economical technique for increasing cavitation intensity would be to reduce the length of the venturi, but for higher volumetric flow rates there could be a limitation due to possibility of flow instability. A similar argument can be given for

enhancement in the cavitation intensity by reducing the venturi throat to pipe diameter ratio.
3. In case of an orifice flow configuration the most convenient way of controlling the cavitation intensity will be to control the orifice to pipe diameter ratio (basically throttling the discharge of a pump through a valve) but indiscriminate growth of the bubbles downstream of the orifice can lead to splashing and vaporization of the flow.
4. Increasing the pipe size downstream of the orifice is another option to intensify cavitation effects but using pipes of higher size would mean handling higher volumetric flow rates (in order to carry out operation at same cavitation number) and this may increase the fixed cost of processing.

Notation

A area of the mean cavitating flow, m^2
A_o area of the orifice, m^2
A_p area of the pipe, m^2
C_i cavitation number, dimensionless
d diameter of the conduit of the turbulent flow, m
d_p diameter of the pipe in orifice flow, m
f_T total number of oscillations of the turbulent velocity fluctuations, dimensionless
I amplitude of turbulent pressure fluctuations, Pa
k polytropic constant of the bubble contents
L length of the venturi, m
L' length of the region of pressure recovery downstream of the orifice plate, m
l length scale of the eddy in orifice flow, m
n number density of bubbles in the liquid, m^{-3}
p average pressure in the gas–liquid flow, Pa
P_2 recovery pressure downstream of venturi or orifice, Pa
P_{g0} initial gas pressure in the bubble, Pa
P_0 ambient pressure in the liquid at the point of generation of the bubbles, N m^{-2}
P_t pressure in the bulk liquid far from bubble, Pa
P_v vapor pressure of the liquid, Pa
R radius of the bubble, m
R_{max} maximum bubble size reached during radial motion, m
R_0 initial bubble radius, m
t time, s
u fluid velocity, m s^{-1}
$\bar{u}'$ turbulent fluctuating velocity, m s^{-1}
u_p velocity in the pipe past the venturi or orifice, m s^{-1}
U mean velocity of the orifice flow, m s^{-1}
U_o velocity at the orifice, m s^{-1}
u_t velocity at the throat of the venturi, m s^{-1}
V volume of an individual bubble, m^3
x distance coordinate, m

Greek letters

α bubble void fraction of the gas–liquid mixture, dimensionless
α_0 initial bubble void fraction of the gas–liquid mixture, dimensionless
β orifice to pipe diameter ratio, dimensionless
η venturi throat to pipe diameter ratio, dimensionless
μ viscosity of the liquid, Pa s
ρ density of the gas–liquid mixture, kg m^{-3}
ρ_L density of pure liquid, kg m^{-3}
σ surface tension of the liquid, N m^{-1}

Acknowledgements

V.S.M. would like to thank Professor Andrea Prosperetti for his help during this work. A.B.P. acknowledges the funding of the DST (Govt. of India) for the project.

References

Chivate, M. M., & Pandit, A. B. (1993). Effect of sonic and hydrodynamic cavitation on aqueous polymeric solutions. *Indian Chemical Engineer*, *35*, 52–57.

Flynn, H. G. (1975). Cavitation dynamics I: Mathematical formulation. *Journal of the Acoustical Society of America*, *57*, 1379–1396.

Hilgenfeldt, S., Lohse, D., & Brenner, M. P. (1996). Phase diagrams for sonoluminescence. *Physics of Fluids*, *8*(11), 2808–2826.

Joshi, J. B., & Pandit, A. B. (1993). Hydrolysis of fatty oils: Effect of cavitation. *Chemical Engineering Science*, *48*(19), 3440–3442.

Moholkar, V. S., & Pandit, A. B. (1997). Bubble behavior in hydrodynamic cavitation: Effect of turbulence. *A.I.Ch.E. Journal*, *43*(6), 1641–1648.

Plessset, M. S., & Prosperetti, A. (1977). Bubble dynamics and cavitation. *Annual Review of Fluid Mechanics*, *9*, 145–185.

Press, W. H., Teukolsky, S. A., Flannery, B. P., & Vetterling, W. T. (1992). *Numerical recipes.* New York: Cambridge University Press.

Save, S. S., Joshi, J. B., & Pandit, A. B. (1994). Microbial cell disruption-role of cavitation. *Chemical Engineering Journal*, *55*(3), B67–B72.

Save, S. S., Joshi, J. B., & Pandit, A. B. (1997). Microbial cell disruption in hydrodynamic cavitation. *Chemical Engineering Research and Design*, *75*(Part C), 41–49.

Shah, Y. T., Pandit, A. B., & Moholkar, V. S. (1999). *Cavitation reaction engineering*. New York: Plenum Press.

van Wijngaarden, L. (1968). On the equations of motion for mixtures of liquid and gas bubbles. *Journal of Fluid Mechanics*, *33*, 465–474.

van Wijngaarden, L. (1972). One-dimensional flow of liquids containing small gas bubbles. *Annual Review of Fluid Mechanics*, *4*, 369–396.

Wang, Y.-C., & Brennen, C. E. (1998). One-dimensional bubbly cavitating flows through a converging-diverging nozzle. *Transactions of the ASME Journal of Fluids Engineering*, *120*, 166–170.